Light-independent phytoplankton degradation and detoxification of methylmercury in water

Xujun Liang[1,2,3,§], Huan Zhong[4§], Alexander Johs[1§], Pei Lei[4,5§], Jin Zhang[4], Neslihan Taş[6], Lijie Zhang[1], Linduo Zhao[7], Nali Zhu[1], Xixiang Yin[1], Lihong Wang[1], Eddy Y. Zeng[8], Yuxi Gao[9], Jiating Zhao[1,2,10,*], Dale A. Pelletier[11], Eric M. Pierce[1], Baohua, Gu[1,2,*]

[1] Environmental Sciences Division, Oak Ridge National Laboratory, Oak Ridge, TN 37831, USA
[2] Department of Biosystems Engineering and Soil Science, University of Tennessee, Knoxville, TN 37996, USA
[3] College of Natural Resources and Environment, Northwest A&F University, Yangling, Shaanxi 712100, China
[4] State Key Laboratory of Pollution Control and Resources Reuse, School of Environment, Nanjing University, Nanjing 210023, China
[5] School of Environment, Nanjing Normal University, Nanjing 210023, China
[6] Climate and Ecosystem Sciences Division, Lawrence Berkeley National Laboratory, Berkeley, CA 94720, USA
[7] Illinois Sustainable Technology Center, Illinois State Water Survey, Champaign, IL 61820, USA
[8] Guangdong Key Laboratory of Environmental Pollution and Health, School of Environment, Jinan University, Guangzhou 511443, China
[9] Key Laboratory for Biomedical Effects of Nanomaterials and Nanosafety, Institute of High Energy Physics, Chinese Academy of Sciences, Beijing 100049, China
[10] Department of Environmental Science, Zhejiang University, Hangzhou, Zhejiang 310058, China
[11] Biosciences Division, Oak Ridge National Laboratory, Oak Ridge, TN 37831, USA

[§] These authors contributed equally.

*Corresponding authors:

B. Gu; Phone: (865) 574 7286; Email: gub1@ornl.gov

J. Zhao; Phone: (865) 576-4946; Email: zhaojt@ihep.ac.cn

Note to Publisher (not for publication):

Abstract

Phytoplankton serves as a key entry point for the trophic transfer and bioaccumulation of the neurotoxin methylmercury (MeHg) in aquatic food webs. However, it is unclear whether and how phytoplankton itself may degrade and metabolize MeHg in the dark. Using several strains of the freshwater alga *Chlorella vulgaris*, the marine diatom *Chaetoceros gracilis*, and two cyanobacteria (or blue-green algae), we report a light-independent pathway of MeHg degradation in water by phytoplankton, rather than its associated bacteria. About 36–85% of MeHg could be degraded intracellularly to inorganic Hg(II) and/or Hg(0) via dark reactions. Endogenic reactive oxygen species, particularly singlet oxygen, was identified as the main driver of MeHg demethylation. Given the increasing incidence of algal blooms in lakes and marine systems globally, these findings underscore the potential roles of phytoplankton demethylation and detoxification of MeHg in aquatic ecosystems and call for improved modelling and assessment of MeHg bioaccumulation and environmental risks.

Keywords

Mercury, methylmercury degradation, algae, bioaccumulation, reactive oxygen species

[Main text]

Methylmercury (MeHg), a potent neurotoxin, is produced from inorganic mercury (Hg) by a group of anaerobic microorganisms possessing the gene cluster *hgcAB* in the environment [1,2]. MeHg is a global health and environmental concern due to its bioaccumulation and biomagnification in aquatic food webs [3,4]. Trace levels of MeHg in water (at picomolar to low nanomolar concentrations) enter the aquatic food web predominantly via biological uptake by phytoplankton, which is considered one of the largest sinks of MeHg [5-8]. At the base of the food web, phytoplankton, consisting of phototrophic prokaryotic and eukaryotic algae and cyanobacteria, contributes to about half of the global primary productivity [9]. In the marine environment, phytoplankton holds about 13–16% of MeHg [5,6], which can be bioaccumulated and biomagnified up to ten-million fold [6,7], reaching toxic levels in fish [4].

MeHg is known to be degraded through various biotic and abiotic pathways, and most attention so far has been focused on photochemical and microbial demethylation [10]. However, photodegradation is limited to surface waters due to the rapid attenuation of ultraviolet (UV) light, particularly in organic-rich waters during algal blooms [11-13], as UVA (320-400 nm) and UVB (280-320 nm) are the dominant drivers of MeHg photolysis [11,12,14]. The *mer*-mediated pathway usually requires relatively high Hg concentrations (i.e., micromolar) to be induced [10], but most natural waters contain Hg and MeHg concentrations typically at picomolar to low nanomolar ranges [3,5,7]. Certain anaerobic bacteria and methanotrophs were shown to degrade MeHg through *mer*-

72 independent pathways at low MeHg concentrations [15,16], although the significance of these
73 demethylation pathways are yet to be confirmed in natural waters [10]. The potential involvement of
74 phototrophs, however, has been largely discounted, particularly with respect to dark, microbial
75 independent demethylation by phytoplankton in freshwater and seawater. One recent study
76 reported that 6 out of 15 marine microalgae species could degrade MeHg, and the main cause was
77 attributed to either photochemical or bacterial demethylation, or both [14]. Other studies have also
78 implicated the potential involvement of marine and freshwater microalgae in MeHg demethylation
79 [17-27], but most have attributed the activity to non-phototrophic microbial degradation,
80 photochemical degradation, or uncharacterized mechanisms [17-27] (summarized in Supplementary
81 Table 1). Demethylation was also observed in suspended settling particles containing planktonic
82 detritus [28], but little or no demethylation was observed in oligo to mesotrophic waters [29,30]. Hitherto
83 phytoplankton is primarily considered a MeHg bioaccumulator and represents a key entry point for
84 MeHg into aquatic food webs [3,7,31]. The roles and pathways of phytoplankton in degrading MeHg
85 are currently unknown, especially during the dark phase of the diurnal cycle. Here, we present
86 evidence of a light- and microbe-independent pathway of MeHg demethylation by phytoplankton,
87 which degrades MeHg to less toxic mercuric Hg(II) or elemental Hg(0).

88 **Phytoplankton Demethylation and Degradation Products**

89 Five phytoplankton species representing common primary producers in aquatic systems [32-
90 34] were examined initially for the degradation of MeHg in the dark. They include the green

91 eukaryotic microalga *Chlorella vulgaris* (CV395 and CV2338), two cyanobacteria, *Synechocystis*
92 *sp.* and *Microcystis sp.* (also known as blue-green algae), from freshwater environments [33], and
93 one marine diatom *Chaetoceros gracilis* (CG2658) [34]. All phytoplankton species tested degraded
94 MeHg in the dark at an initial MeHg concentration of 25 nM (Fig. 1A). The diatom CG2658
95 displayed the highest rate (~0.040 h^{-1}) and magnitude of demethylation with more than 85% of
96 MeHg converted to Hg(II) or Hg(0) after 5 days in the dark (Fig. 1A; Supplementary Table 2).
97 Extensive degradation of MeHg (~70%) was also observed with CV395 cells after 5 days, with an
98 estimated demethylation rate of 0.017 h^{-1}. Like CV395 and CG2658, the cyanobacterium
99 *Synechocystis* sp. degraded ~75% of MeHg after 5 days, and the demethylation rate constant was
100 ~0.016 h^{-1} (Fig. 1A; Supplementary Table 2). *Microcystis* sp. degraded ~50% of MeHg, lower than
101 other phytoplankton species under the same experimental conditions. As expected, negligible
102 amounts of MeHg (< 6%) were degraded abiotically in the dark in simulated freshwater (SFW) or
103 simulated seawater (SSW) (i.e., no-cell controls), or in the cell filtrates (< 0.2 μm), or with heat-
104 killed CV cells (Fig. 1B), suggesting that metabolically active phytoplankton cells were necessary
105 for demethylation. The degradation products appeared species-specific, being identified mainly as
106 elemental Hg(0) by CG2658 and cyanobacteria (Extended Data Fig. 1) or as Hg(II) by CV395.
107 This observation may be attributed to a relatively high cellular thiol content of CV cells (~165
108 amol·$cell^{-1}$), as thiolates are known to mediate Hg(0) oxidation to Hg(II) in the dark [35,36]. CG2658
109 contained only about 88 amol·$cell^{-1}$ thiols (Supplementary Fig. S2). Similarly, the genome of

110 CV395 showed a higher fraction of cysteine residues, approximately 80% greater than those found
111 in the cyanobacteria *Synechocystis* sp. and *Microcystis* sp. (Supplementary Table S3).

112 These initial findings demonstrate that certain phytoplankton species can degrade MeHg to
113 Hg(0) or Hg(II) in the dark at relatively high concentrations of MeHg (25 nM) and phytoplankton
114 cells (1×10^6 mL^{-1}), although the ratio of MeHg to cells is within the range observed in aquatic
115 environments (0.002-162 amol MeHg/cells) [37-39] (Supplementary Table S1). To further validate
116 whether demethylation occurs under more environmentally relevant conditions, e.g., lower cell
117 density, low MeHg concentrations and typical diel dark/light settings, additional assays were
118 performed using CV as one of the most prevalent green algae in freshwater [32]. The experiments
119 were carried out independently with a different CV strain (CV2338), obtained from the Freshwater
120 Algae Culture Collection (FACHB) at the Institute of Hydrobiology in China, at MeHg
121 concentrations of either 0.05 nM (Fig. 1C,D) or 0.001 nM (Fig. 5D, described below) and a cell
122 density of 10^5 cells mL^{-1}, as observed during algal blooms [5,7,40]. Under these experimental
123 conditions, we also observed substantial degradation of MeHg in the dark: ~40 and 72%
124 demethylation occurred in 72 h with an estimated rate constant of 0.049 h^{-1} and 0.031 h^{-1} at the
125 initial MeHg concentrations of 0.05 and 0.001 nM, respectively (Supplementary Table S2). Again,
126 negligible amounts of MeHg degradation (< 4%) were found in control samples, including SFW,
127 CV filtrate (< 0.2 μm), and heat-killed CV cells (Fig. 1D), evident that the presence of live CV
128 cells is necessary for demethylation to occur. The observed demethylation cannot be attributed to

129 phytoplankton growth, as we found little or no growth of CV cells during the 5-day reaction period
130 (Supplementary Fig. S4). Meanwhile, key indicators related to phytoplankton physiology, i.e., cell
131 morphology, malondialdehyde concentrations (indicative of cell oxidative damage in the dark) [41,42],
132 and dissolved oxygen levels, were not affected significantly during the 5-day dark incubation
133 (Supplementary Fig. S5). These results are consistent with previous observations, indicating that
134 prolonged darkness has no significant impact on cell density, chlorophyll-*a* content, cell surface
135 area and volume [43]. Additionally, similar rates and extent of demethylation were observed between
136 experiments performed under 24-h dark or under 12-h dark+12-h light conditions ($p > 0.05$,
137 Supplementary Fig. S3), further supporting potential occurrences of phytoplankton demethylation
138 in water.

139 To obtain additional confirmation and insight into the degradation of MeHg by
140 phytoplankton, we examined whether or not demethylation occurred intracellularly by determining
141 the uptake and distribution of MeHg and its degradation products, i.e., inorganic Hg(II) and Hg(0)
142 by CV cells (Fig. 2). Results show that a significant fraction of MeHg (11–46%) was adsorbed on
143 the CV cell surface, and 16–40% of MeHg was taken up intracellularly in the dark at relatively
144 high MeHg and CV concentrations (Fig. 2A). In experiments with low concentrations of MeHg
145 (0.05 nM) and CV (10^5 cells mL^{-1}), more MeHg (~70%) was taken up intracellularly within 6 h
146 (Fig. 2B), due to a decreased MeHg-to-CV cell ratio and thus a lower amount of MeHg adsorbed
147 on cell surfaces, as previously observed [7,31]. In both cases, the adsorption and uptake of MeHg

148 resulted in <10% of MeHg remaining in solution (Fig. 2). Meanwhile, the intracellular MeHg
149 ($MeHg_{int}$) decreased over time, resulting in a concurrent increase in the intracellular inorganic Hg
150 [$Hg(II)_{int}$], with negligible amounts of adsorbed inorganic Hg [$Hg(II)_{ads}$] and soluble $Hg(II)_{sol}$ (Fig.
151 2). Small amounts of MeHg were converted to elemental Hg(0) in experiments with relatively high
152 MeHg and CV concentrations (Fig. 2A). After 5 days, about 65 and 40% of MeHg were degraded
153 and converted to $Hg(II)_{int}$, respectively, in the high and low MeHg/CV concentration experiments
154 (Fig. 2). These observations suggest that MeHg was taken up and then degraded to Hg(II) or Hg(0)
155 intracellularly by CV cells in the dark.

156 **Demethylation is not Caused by Bacteria**

157 Bacteria associated with phytoplankton could potentially contribute to the observed
158 demethylation, as certain aerobic and anaerobic bacteria are known to degrade MeHg [10]. To
159 ascertain that the observed demethylation is attributable to phytoplankton cells, multiple control
160 experiments and 16S rRNA analyses were performed. These complementary lines of evidence
161 confirmed that MeHg degradation was indeed caused by phytoplankton itself, rather than
162 associated bacteria.

163 First, we conducted 16S rRNA analyses of both CV and CG cultures and their filtrates (<
164 3 μm) targeting alphaproteobacteria and gammaproteobacteria, as they are among the most
165 commonly observed algal symbionts with the potential to degrade MeHg [44-46]. The initial screening
166 indeed showed the presence of both alphaproteobacteria and gammaproteobacteria in the culture

and the 3-μm filtrate samples of CG2658 and CV395 samples. However, despite the presence of these bacteria in the 3-μm filtrates, demethylation was not observed in the CG or CV filtrate samples at either high or low MeHg concentrations (Fig. 3A,B). Furthermore, when the CV filtrate (<3 μm) or live cells were rested for 5 days at room temperature (presumably allowing more bacteria to grow) before incubation with MeHg, we again observed no significant demethylation in the CV filtrate but ~40% lower amounts of MeHg degraded by the rested CV cells (Fig. 3C). These results clearly indicate that bacteria were not the primary driver of demethylation when phytoplankton cells were inactivated or removed.

Second, independent demethylation assays confirmed the degradation of MeHg by the CV2338 strain (Figs. 1C, 3D), while 16S rDNA gel electrophoresis and scanning electron microscopy (SEM) analyses showed the absence of bacterial contamination in these samples (Supplementary Fig. S6). Additionally, demethylation rates (0.049 to 1.50 h^{-1}) by CV2338 and its cell lysate (Fig. 3D and Supplementary Table S2) were much higher than those typically reported for bacterial demethylation in laboratory cultures and field incubations (0.001–0.079 h^{-1}) [16-18,20,47,48]. Within a short time period (1 h), a high percentage of MeHg (45%) was degraded in the CV2338 cell lysate (Fig. 3D). Moreover, MeHg degradation increased only slightly to ~55% at 6 h and to 64% at 72 h (Fig. 3D). This initial rapid degradation of MeHg by the phytoplankton cell lysate is inconsistent with the commonly observed demethylation dynamics by bacteria [10,49], suggesting that microbial contamination was not the primary driver of the observed phytoplankton demethylation.

186 Lastly, demethylation by aerobic bacteria usually requires relatively high Hg(II) or MeHg
187 concentrations (i.e., micromolar) to be effective via the Hg resistance (*mer*) pathway [10,49]. The
188 observed demethylation by phytoplankton cells at MeHg concentrations of picomolar levels (i.e.,
189 1-50 pM, Fig. 1C; 3D) does not support *mer*-mediated demethylation observed in previous studies
190 (described below) [48]. Although demethylation by anaerobic bacteria and methanotrophs at low
191 MeHg concentrations has been documented [15,16,47], our experiments were performed under oxic
192 conditions and showed that the presence of live phytoplankton cells was required to observe
193 demethylation (Figs. 1 and 3). Therefore, multiple lines of experimental evidence corroborate our
194 findings that phytoplankton cells degrade MeHg in the dark using a mechanism that is different
195 from recognized microbial demethylation pathways [10,49].

196 **Potential Mechanisms of Phytoplankton Demethylation**

197 In search for the potential mechanism involved in phytoplankton demethylation, we
198 considered whether genes with functions similar to the Hg-resistance pathway exist in
199 phytoplankton. The broad-spectrum *mer* operons include two key enzymes, an organo-mercurial
200 lyase (MerB), which cleaves the C-Hg bond, and mercuric reductase (MerA), which reduces Hg(II)
201 to Hg(0) [10,49]. While no gene homologous to MerB was detected in any phytoplankton genomes,
202 homologs of MerA and the metal-responsive transcriptional regulator MerR were identified
203 (Supplementary Table S4). Although MerA homologs show ~30% sequence identity
204 (Supplementary Table S5) to the well-characterized MerA from plasmid pDU1358 [50], a multiple

sequence alignment (Supplementary Fig. S7) indicates important differences to canonical MerAs. While three key residues essential for the function of MerA are conserved, they all lack metallochaperone domains (NmerA) [51], a C-terminal vicinal cysteine pair and two tyrosine residues implicated with Hg(II) handoff (Supplementary Fig. S7) [52].

The absence of other genes related to Hg resistance, specifically *mer*B, *mer*T, or *mer*D, further confirms that complete *mer* operons are absent (Supplementary Table S4). Moreover, the canonical *mer* operon was not found among the cyanobacteria, the Bacillariophyta (diatoms), and the Viridiplantae, which include all eukaryotic algae. Therefore, the observed MeHg degradation by phytoplankton in this study involves a novel mechanism distinct from the *mer*-mediated demethylation.

We next considered the potential involvement of reactive oxygen species (ROS), such as singlet oxygen ($^1O_2$), superoxide anions ($O_2^{-}\cdot$), and hydroxyl radicals ($\cdot OH$), in phytoplankton demethylation, as dark production of ROS, such as $^1O_2$ and $O_2^{-}\cdot$, is recognized among marine diatoms, cyanobacteria, and eukaryotes [53,54]. Photochemically produced ROS, such as $^1O_2$, are also demonstrated to drive abiotic photodemethylation in both laboratory and field studies [10,11,55,56]. Therefore, we hypothesize that the mechanism of phytoplankton demethylation is mediated directly by intracellular ROS following the internalization of MeHg by the cells. To test this hypothesis, we measured dark demethylation with CV cell lysate using the well-established scavenger technique [53,55,57,58]. ROS scavengers were selected based on their specificity, broad use

224 in biological systems, and minimal interferences in MeHg analysis. Here β-carotene was used as a
225 scavenger for $^1O_2$, as it is an endogenous compound in phytoplankton and known to have minimal
226 impact on cellular functions [57]. An additional scavenger, 2,5-dimethylfuran, was used to confirm
227 the role of $^1O_2$ in phytoplankton demethylation [58]. Superoxide dismutase (SOD) and ethyl alcohol,
228 endogenously produced in phytoplankton cells as well, were used to scavenge $O_2^{-}\cdot$ and ·OH
229 radicals, respectively [53,55,58]. Results show that scavenging $^1O_2$ by either β-carotene or 2,5-
230 dimethylfuran (Fig. 4A; Supplementary Fig. S8) resulted in the most dramatic effect, in which no
231 significant demethylation was observed, as compared to 33% (1 h) and 44% (6 h) of MeHg
232 degradation without the scavenger added to the CV cell lysate (Fig. 4A). Scavenging $O_2^{-}\cdot$ by SOD
233 showed only minor effects in inhibiting MeHg degradation (~15% in 6 h) (Fig. 4A and
234 Supplementary Fig. S8, $p < 0.05$). In contrast, scavenging ·OH had no effects on demethylation
235 (Fig. 4A). As expected, the scavengers themselves did not induce MeHg degradation (Fig. 4B), as
236 previously reported [58].

237 Inhibited demethylation by the scavenger addition clearly shows the potential role of $^1O_2$
238 and $O_2^{-}\cdot$ in MeHg degradation by CV cells. Additional support was obtained from confocal
239 microscopy, indicating spatially coupled reactions between MeHg and $^1O_2$ in live CV cells. The
240 production of $^1O_2$ was visualized intracellularly both in the whole cell (green channel) (Fig. 4C)
241 and in $^1O_2$-generating organelles (indicated by acridine orange-labeled DNA) in the dark (Fig. 4D).
242 Upon MeHg exposure, the fluorescence signal of Hg (blue channel) appeared to be co-located with

243 $^1O_2$ (green channel) (Fig. 4C, overlay images). The two-channel colocation scatter plots yielded a
244 Pearson correlation coefficient (r_p) of ≥ 0.7 (Fig. 4C). Meanwhile, continuous production of $^1O_2$
245 was found in either intact cells or their lysates (Supplementary Figs. S9–S10), irrespective of light
246 and dark incubations (from 1 h to 120 h) or ultrasonication (for preparing cell lysates). Together
247 with the observed rapid demethylation kinetics (Figs. 1A,C and 3D) or inhibited demethylation by
248 $^1O_2$ scavengers (Fig. 4A,B), these results offer a plausible explanation of ROS-mediated
249 demethylation by phytoplankton.

250 Intracellular thiols have also been shown to facilitate the breakdown of MeHg under $^1O_2$
251 attack [55], as thiols can form strong complexes with MeHg and thus weaken the C-Hg bond [55,59].
252 However, other studies suggest that thiols may react with ROS alleviating oxidative stress at the
253 cellular level [60,61]. Conceivably, cellular thiol contents and the balance between the production and
254 consumption of endogenous ROS likely determine how much MeHg is degraded by the
255 phytoplankton. We also note that since CV was used as one of the representative phytoplankton
256 species and a model microalga, different phytoplankton species may exhibit different MeHg uptake
257 and demethylation rates with metabolically different degradation pathways and products.
258 Furthermore, some phytoplankton species may not degrade MeHg, as previously reported [14], and
259 degradation can be affected by environmental conditions. We therefore suggest that, while our
260 study provided the first step in understanding the pathway of light-independent phytoplankton
261 demethylation, future studies are warranted to ascertain the direct involvement of intracellular ROS

and its environmental significance in biological dark demethylation (e.g., its relative importance compared to other microbial demethylation pathways).

Phytoplankton Demethylation in Natural Water and Implications

To provide an additional environmental perspective of phytoplankton demethylation, we determined MeHg degradation in natural waters collected from (a) Melton Lake in Oak Ridge, Tennessee, United States, (b) Yangshan Lake in Nanjing, China, and (c) the North Pacific Ocean in Venice, California. Water samples were filter-sterilized through 0.2-μm filters, or otherwise stated, before incubation either with or without CV or CG cells in the dark. In all experiments, little or no demethylation was observed without the addition of CV or CG cells (Fig. 5). However, the addition of phytoplankton cells substantially increased MeHg degradation, particularly in the presence of CG in North Pacific seawater (Fig. 5A). At relatively high concentrations of MeHg (25 nM) and phytoplankton (1×10^6 cells mL^{-1}), about 40% and 90% of MeHg were degraded by CV395 in the Melton lake water and by CG in North Pacific seawater (Fig. 5A, B), respectively, as compared to <5% of MeHg degraded in 5 days in the absence of phytoplankton. Similarly, as observed in the simulated seawater (Supplementary Fig. S1), most MeHg was converted to Hg(0) by CG in the dark but to a lesser extent by CV395 cells (Supplementary Fig. S11). In experiments at low concentrations of MeHg (0.05 and 0.001 nM) and phytoplankton (1×10^5 cells mL^{-1}), the presence of CV2338 resulted in 70–80% of MeHg degradation in Yangshan Lake water in 72 h (Fig. 5C, D). This observation could not be attributed to microbes in the lake water, as experiments

281 with the filtered and unfiltered lake waters showed similar demethylation rates by CV cells in the
282 dark (Supplementary Fig. S12). However, the addition of alga-derived organic matter (AOM), as
283 a major DOM component in eutrophic lake water [62], slightly decreased MeHg degradation by
284 CV2338 (to 49% in 72 h) in Yangshan Lake water (Fig. 5C). This result is not surprising, as AOM
285 could form complexes with MeHg and thus slow down cell sorption and uptake of MeHg [23,63,64].
286 However, once inside the cell (within 24 h), most MeHg was degraded in 72 h (~90% without
287 AOM versus 85% with AOM, Supplementary Fig. S13). These results again illustrate the important
288 roles of phytoplankton in degrading MeHg in natural waters, even in the presence of relatively high
289 concentrations of AOM (14.3 mg C/L) [62].

290 Overall, the observed phytoplankton demethylation exemplifies a previously overlooked
291 MeHg degradation pathway that is light-independent and distinct from other described microbial
292 degradation mechanisms. The pathway involves the cleavage of the C-Hg bond by endogenic ROS,
293 such as $^1O_2$, a mechanism that is different from the *mer*-mediated detoxification pathway.
294 Phytoplankton not only takes up MeHg rapidly but also acts as a MeHg degrader by breaking it
295 down to inorganic Hg(II) or elemental Hg(0) in the dark, thereby decreasing MeHg
296 bioaccumulation and trophic transfer in aquatic food webs. Recognition of this pathway and its
297 impact on the net MeHg budget and its bioaccumulation is significant, considering that
298 phytoplankton is one of the primary sinks of MeHg in both photic and aphotic water bodies [5,6,31].
299 As a first step, these findings could lay the foundation for future studies in elucidating detailed

mechanisms and implications underpinning the observed phytoplankton demethylation and help refine models by incorporating phytoplankton demethylation for improved prediction of MeHg bioaccumulation. Our findings imply that phytoplankton may absorb more MeHg than that suggested by current measurements and models [5,6,8], which do not account for phytoplankton demethylation. The rates used in previous models only represent the net uptake rates, much lower than the actual gross uptake, as our study suggests that 36–85% of MeHg could be degraded intracellularly. Further laboratory and field studies are therefore necessary to better understand specific phytoplankton species and environmental conditions (e.g., temperature, DOM, irradiation, etc.) responsible for demethylation. Such studies are essential for determining the extent that marine and freshwater microalgae may be involved in uptake and demethylation observed in previous field and laboratory studies [14,17-27] and defining their roles compared to photochemical and non-phototrophic microbial demethylation. Given the widespread presence of phytoplankton and worldwide increasing incidences of algal blooms under climate change [34,65], an improved understanding of phytoplankton demethylation can aid in better predicting trophic transfer and global cycling of Hg.

Online content

Any methods, additional references, Supplementary information, acknowledgements; details of author contributions and competing interests; and statements of data availability are available at xxxxxx.

Methods

Phytoplankton Cultures and Assay Media. *Chlorella vulgaris* UTEX 395 (abbreviated as CV395) and *Chaetoceros gracilis* UTEX 2658 (abbreviated as CG2658) were obtained from the Culture Collection of Algae, University of Texas at Austin, United States. One additional strain of *Chlorella vulgaris* 2338 (abbreviated as CV2338) and two freshwater cyanobacteria (*Microcystis* sp. 0824 and *Synechocystis* sp. PCC6803) were obtained from the Freshwater Algae Culture Collection (FACHB) at the Institute of Hydrobiology, China. These taxa were used to represent algae and cyanobacteria frequently found in aquatic environments [32-34] and are widely used in biogeochemical transformation studies of Hg [59,64,66]. All freshwater algae and cyanobacteria were cultured in UTEX BG-11 medium, whereas *Chaetoceros gracilis* was grown in UTEX Erdschreiber medium at 23 °C under cool white fluorescent lamps for 16 h per day at a light intensity of ~50 μmol photons m^{-2} s^{-1}. The media composition is available at https://utex.org/collections/all-products. Cells were harvested at the mid-exponential phase (after ~20 d) and washed three times with and resuspended in the simulated freshwater (SFW) or simulated seawater (SSW, for *Chaetoceros gracilis*). The chemical compositions of SFW or SSW are listed in Supplementary Table S6.

Natural freshwater and marine water samples were collected and used for demethylation assays either in the presence or absence of phytoplankton. They include (a) Melton Lake water collected from Oak Ridge, Tennessee, United States, (b) Yangshan Lake water from Nanjing,

China, and (c) seawater from the North Pacific Ocean at Venice, California, United States. The geochemical properties of these natural waters are listed in Supplementary Table S6. All natural water samples were filter-sterilized through 0.2-μm Acrodisc syringe filters (Pall Corporation) before use or otherwise specified. In all experiments, phytoplankton cells were washed with the respective assay media (i.e., SFW, SSW, or natural water), and the washed cell suspension was then rested in the dark for ~20 h at 23 °C before demethylation assays. For selected experiments, two aliquots of the cell suspensions (50 mL each) were filtered through either 0.2-μm or 3.0-μm syringe filters to obtain the < 0.2 μm and < 3 μm cell filtrates, respectively. An additional aliquot (50 mL) was heated to 80 °C for 60 min to obtain heat-killed cells. All these cell filtrates, the heat-killed cells, SFW, SSW, and unfiltered or filtered natural waters, were used as controls in demethylation assays.

Assays. Demethylation was performed by mixing the cell suspension with MeHg to give a final cell density of either 1×10^6 or 1×10^5 cells mL^{-1} and a MeHg concentration of 25 nM, 0.05, or 0.001 nM in glass vials (Thermo Scientific). As a common laboratory practice, small sample volumes were used in demethylation assays to minimize hazardous waste generation while maintaining ratios of MeHg to phytoplankton cells similar to those observed in natural systems. Environmentally relevant concentrations of MeHg (0.001 and 0.05 nM) and phytoplankton cells (1×10^5 cells mL^{-1}) were used to represent the range that is observed in natural waters [37-39] and/or used in previous studies [5,7,23,64]. Similarly, an incubation temperature of 28 °C was used to mimic

357 the water temperature observed in summer months during algal blooms, for example, in Lake
358 Taihu, China, with ~1/4 of the monthly temperatures above 26 °C [67], as well as in the Laurentian
359 Great Lakes and many other lakes [68,69]. The MeHg working solution was prepared from a 5 μM
360 stock solution (Brooks Rand Inc.) in either SFW, SSW, or filtered natural waters. All vials were
361 acid-washed and combusted at 450°C for 4.5 h before use. The vials were sealed with PTFE-lined
362 silicone screw caps, and samples were incubated either in the dark (covered with aluminum foil)
363 for up to 5 days, or otherwise specified. At selected time points (1–120 h), 2–4 sample vials were
364 taken out of the incubator and analyzed for the total remaining MeHg and its degradation products,
365 inorganic Hg(0) or Hg(II) species, as described in details below. All control experiments with heat-
366 killed cells, cell filtrates, SFW, SSW, and natural waters were performed in the same manner.

367 To confirm that demethylation was not caused by bacteria, which may be present in
368 phytoplankton cultures, selected assay samples were subjected to 16S rDNA and DNA
369 electrophoresis analyses before and after incubation. The hypervariable regions of bacterial 16S
370 rDNA genes were targeted for analysis. The total community DNA extraction was performed using
371 an Ezup Column Bacteria Genomic DNA Purification Kit (Sangon Biotech Co., Shanghai, China)
372 following the manufacturer's instructions [70]. Two universal amplicon PCR primers, 27F
373 (AGAGTTTGATCMTGGCTCAG) and 1492R (GGTTACCTTGTTACGACTT), covering nearly
374 full-length of 16S rDNA for Gram-positive and Gram-negative bacteria, were used to amplify the
375 gene sequence of potential bacterial communities [71,72]. The PCR amplification was performed

immediately following DNA extraction in a 25 μL reaction mixture containing 2×PCR buffer, dNTP (each 10 mM), Taq Plus DNA Polymerase (5 U/μL), 50 mM $MgSO_4$ (12.5 μL), primer F (10 μM, 1 μL), primer R (10 μM, 1μL), template DNA (1 μL), and deionized water (9.5 μL). PCR was determined on a thermal cycler (Applied Biosystems 9700, USA) as follows: 1 cycle of denaturing at 95 °C for 5 min, 1 cycle of 94 °C for 30 s, 30 cycles of annealing at 57 °C for 30 s, 72 °C for 90 s, and a final extension step at 72 °C for 10 min. The extracted DNA and PCR products were further examined and validated using electrophoresis in 1.5 % (w/v) agarose gels in TAE buffer, stained with ethidium bromide, and visualized under UV light.

Hg and MeHg Species Distributions. Experiments were performed to determine MeHg and its degradation product inorganic Hg species distributions (e.g., dissolved vs. adsorbed Hg or MeHg on cell particulates) during demethylation assays, as previously described [16,73]. Briefly, a total of six sample vials were taken, and elemental Hg(0) concentrations were determined first by directly purging and analyzing Hg(0) using a Zeeman cold vapor atomic absorption spectrometer (CVAAS, RA-915+ analyzer, Ohio Lumex Company). Two samples were then filtered directly through 0.2-μm Acrodisc® syringe filters (13 mm diameter, Pall Corporation) to remove cell particulates, and the filtrates were assayed for the non-purgeable soluble Hg ($HgNP_{sol}$) and MeHg ($MeHg_{sol}$). $HgNP_{sol}$ was analyzed after the sample was oxidized in BrCl (described below) so that the soluble inorganic Hg(II) [$Hg(II)_{sol}$] could be determined by the difference between $HgNP_{sol}$ and $MeHg_{sol}$. Another two samples (unfiltered) were analyzed for the total non-purgeable Hg (THg_{NP})

and MeHg (TMeHg). The remaining two samples were reacted with 150 μM 2,3-dimercapto-1-propanesulfonic acid (DMPS), a strong Hg-chelating agent [73], for 15 min to wash off the cell surface-adsorbed inorganic Hg(II) [$Hg(II)_{ads}$)] and $MeHg_{ads}$. These samples were again filtered, the filtrates analyzed for DMPS-soluble $HgNP_{Dsol}$ and $MeHg_{Dsol}$, and the adsorbed $MeHg_{ads}$ was determined by the difference between $MeHg_{Dsol}$ and $MeHg_{sol}$. MeHg uptake or the intracellular MeHg [$MeHg_{int}$] was determined by subtracting $MeHg_{Dsol}$ from TmeHg (i.e., $MeHg_{int}$ = TmeHg – $MeHg_{Dsol}$). Similarly, the adsorbed $Hg(II)_{ads}$ was estimated by subtracting $Hg(II)_{sol}$ and $MeHg_{Dsol}$ from $HgNP_{Dsol}$, and the intracellular Hg(II) [$Ihg(II)_{int}$] determined by subtracting $HgNP_{Dsol}$ and $MeHg_{int}$ from THg_{NP} (i.e., $Ihg(II)_{int} = THg_{NP} – HgNP_{Dsol} – MeHg_{int}$) [16,73].

Hg Resistance Gene Analysis. Genome sequence data and individual protein sequences of *Synechocystis* sp. PCC6803 and *Microcystis* sp. 0824 were obtained from UniProtKB [74] and the JGI Genome Portal [75,76]. The assembled genomic scaffolds for CV were obtained from a draft genome released by the *Chlorella vulgaris* Genome Project [77]. *Chaetoceros gracilis* and CV 2338 were excluded from the genomic analysis since no complete genomes were available. The Basic Local Alignment Search Tool (BLAST) was used to search for candidate gene products with sequence similarity to template protein sequences, including the organomercurial lyase MerB (GenBank: AAA88369), the mercuric reductase MerA (GenBank: ADM52740), the transcriptional regulator MerR (GenBank: AAA98221), the transcriptional repressor MerD (GenBank: AAA88370), and mercuric ion transporter MerT (GenBank: AAA98222) [50,78]. A set of known

414 mercuric reductases (MerA) genes were aligned with the identified homologs using Clustal Omega
415 [79]. Jalview 2.10.5 was used to visualize multiple sequence alignments [80].

416 **Roles of ROS.** To determine whether ROS played a role in MeHg degradation by
417 phytoplankton, similar demethylation assays were performed with the CV2338 lysate using
418 previously established scavenger addition methods [55,58,81]. Briefly, the CV lysate was obtained by
419 ultrasonication at 520 W for 5 min with an on-and-off cycle of 5 s in an ice bath and then diluted
420 in SFW to an equivalent of the cell density of 1×10^5 cells mL^{-1}. Demethylation assays were initiated
421 by adding MeHg (0.05 nM) and appropriate radical scavengers at 28 °C in the dark. At selected
422 time points, the MeHg remaining in the suspension was analyzed, as described earlier. *β*-carotene,
423 2,5-dimethylfuran, ethanol, and superoxide dismutase enzymes (SOD) were used to scavenge the
424 production of singlet oxygen ($^1O_2$), hydroxyl (·OH), and superoxide ($O_2^{-\cdot}$), respectively [55,58,81]. The
425 added scavenger concentrations were as follows: 10 mM *β*-carotene or 2,5-dimethylfuran, 100 mM
426 ethanol, or 1 mg L^{-1} SOD, as previously described [58]. Control samples were prepared similarly
427 either in the CV lysate without added scavengers or in the scavenger without added CV lysate.

428 The spatial coupling between MeHg and singlet oxygen (based on their fluorescence
429 signals) was explored with live CV2338 cells [82-84]. Briefly, CV2338 cells were concentrated and
430 resuspended in PBS (with a final cell density of about 1.5×10^8 cells mL^{-1}). Then, about 2.5 μM
431 MeHg was spiked into the suspension and reacted for 30 min. Fluorescent probes of Pep2-TPE [82],
432 Singlet Oxygen Sensor Green (SOSG) [83,85], and Acridine Orange [84], were used to label MeHg (as

433 Hg), singlet oxygen, and DNA in live cells, respectively. The fluorescence signal was then recorded
434 using a confocal laser scanning microscope (Zeiss LSM880 with Airyscan). Images were analyzed
435 using the software ImageJ, and colocalization analysis was performed as previously described [86,87].
436 **Hg and MeHg Analytical Methods.** After purging and CVAAS analysis of Hg(0), an
437 aliquot from each vial was taken for MeHg analysis, and the remaining sample was oxidized in
438 BrCl (5%, v/v) at 4 °C overnight or longer and analyzed for total non-purgeable Hg(II) (HgNP) via
439 $SnCl_2$ reduction and detection by CVAAS [16,73,88]. Hg(0) and Hg(II) concentrations were quantified
440 using external calibration curves, and the detection limit was ~10 pg Hg. The total Hg concentration
441 was calculated by summating the purgeable Hg(0) and HgNP, and a good mass balance was
442 obtained (usually within 97–110%). For MeHg analysis, an aliquot of 25–100 μL (depending on
443 sample concentrations) was transferred into a distillation container prefilled with ~40 mL Milli-Q
444 water and placed on a Tekran (Model 2750) distillation apparatus (EPA Method 1630) [1,2,36]. A
445 known amount of isotopically labeled $Me^{200}Hg$ was added to each distillation vial as an internal
446 standard to correct potential loss of MeHg during distillation [16,36]. Following the distillation, MeHg
447 was ethylated and analyzed by purging and trapping onto a Tenax trap, followed by thermal
448 desorption and separation using an automated MERX-M system (Brooks Rand Instruments), and
449 detection by an inductively coupled plasma mass spectrometer (ICP-MS) (Elan DRC-e,
450 PerkinElmer) [1,16]. Randomly selected samples spiked with known amounts of MeHg standards

were run with every batch of samples for quality assurance and quality control (QA/QC). The recovery of spiked MeHg standards was 100±10%, and the detection limit was ~ 6 pg Hg.

Data Availability

All study data are included in the article and/or Supplementary.

Acknowledgments

We thank Xiangping Yin and Zhuoran Li for technical assistance in experiments and biochemical analyses. This research was supported in part by the Office of Biological and Environmental Research within the Office of Science of the U.S. Department of Energy (DOE), as part of the Critical Interfaces Science Focus Area project at Oak Ridge National Laboratory (ORNL), and by the National Natural Science Foundation of China (12222509, 42107383) and the Natural Science Foundation of Jiangsu Province (BK20200322). The DOE will provide public access to these results of federally sponsored research in accordance with the DOE Public Access Plan (http://energy.gov/downloads/doe-public-access-plan). ORNL is managed by UT-Battelle, LLC under Contract No. DE-AC05-00OR22725 with DOE.

Author Contributions Statement

xxxx.

Competing Interests Statement

The authors declare no competing interests.

Additional information

Supplementary information for this paper is available at https://doi.org/xxxxxx.

Correspondence and requests for materials should be addressed to Baohua Gu and Jiating Zhao.

Figure Legends

Fig. 1. Dark degradation of methylmercury (MeHg) by phytoplankton *Chlorella vulgaris* CV395, *Chaetoceros gracilis* CG2658, *Synechocystis* sp. PCC6803 (Syn), and *Microcystis* sp. 0824 (Mic) (A), and *Chlorella vulgaris* CV2338 (C), and their respective cell filtrates (<0.2-μm) and heat-killed CV cells as abiotic controls (B, D). Experiments performed either at high concentrations of MeHg (25 nM) and phytoplankton cells (1×10^6 cells mL^{-1}) (A, B) or at low concentrations of MeHg (0.05 nM) and phytoplankton cells (1×10^5 cells mL^{-1}) (C, D). Simulated freshwater (SFW) was used in experiments with CV395, PCC6803, sp. 0824, and CV2338, whereas simulated seawater (SSW) was used in experiments with CG2658 (see Methods for details). Data represent averages from 2–4 replicate samples with error bars showing one standard deviation.

Fig. 2. Hg species distributions during methylmercury (MeHg) degradation in the dark. Demethylation by (A) C*hlorella vulgaris* CV395 at the initial MeHg concentration of 25 nM and CV concentration of 1×10^6 cells mL^{-1} and (B) by *Chlorella vulgaris* CV2338 at the MeHg concentration of 0.05 nM and CV concentration of 1×10^5 cells mL^{-1}. $MeHg_{int}$, $MeHg_{ads}$, and $MeHg_{sol}$ represent the intracellular, adsorbed, and soluble MeHg, respectively, whereas Hg(0), $Hg(II)_{int}$, $Hg(II)_{ads}$, and $Hg(II)_{sol}$ represent elemental Hg(0), the intracellular, adsorbed, and soluble inorganic Hg(II) species, respectively (see Methods for details). Data represent averages from 2–4 replicate samples with error bars showing one standard deviation.

Fig. 3. Methylmercury (MeHg) degradation during dark incubation with cell filtrates (<3 μm) of *Chlorella vulgaris* CV395 and *Chaetoceros gracilis* CG2658 at relatively high concentrations of MeHg (25 nM) and phytoplankton cells (1×10^6 mL^{-1}) (A), or at low concentrations of MeHg (0.05 nM) and *Chlorella vulgaris* CV2338 cells (1×10^5 cells mL^{-1}) (B, C, D). (B) CV cell filtrate (<3 μm), (C) live CV and its filtrate rested for 5 days before demethylation, and (D) live CV and cell lysate. Cell filtrates were obtained by filtering and removing an equivalent amount of live cells through 3-μm syringe filters. Data represent averages from 2–4 replicate samples with error bars showing one standard deviation.

Fig. 4. Evaluation of reactive oxygen species (ROS), including singlet oxygen ($^1O_2$), superoxide ($O_2^{-}\cdot$), and hydroxyl (·OH) radicals, on dark degradation of methylmercury (MeHg, 0.05 nM) in (A) the cell lysate of *Chlorella vulgaris* CV2338, or (B) in simulated freshwater (SFW) with or without added ROS scavengers (see Methods for details). Spatial coupling of the fluorescence signal of methylmercury (MeHg) and singlet oxygen (C) or DNA (D) in live *Chlorella vulgaris* CV2338 cells. Columns from left to right: blue channel (MeHg), green channel (singlet oxygen), red channel (DNA), overlay images, and two channel colocation scatter plots. Note that the overlay between blue and red channels gave the observed magenta color in (D). The Pearson correlation coefficient r_p was indicated on the scatter plots (see Methods for additional details). Data in (A) and (B) represent averages from 3-4 replicate samples with error bars showing one standard deviation. Different letters (a, b, or c) denote significant differences among different treatments (one-way ANOVA, $p < 0.05$).

Fig. 5. Methylmercury (MeHg) degradation either with or without added *Chlorella vulgaris* CV395 cells in Melton Lake water (A) or *Chaetoceros gracilis* CG2658 cells in Venice seawater (B) in the dark at high concentrations of MeHg (25 nM) and cell density (1×10^6 cells mL^{-1}). MeHg degradation either with or without added *Chlorella vulgaris* CV2338 cells (1×10^5 cells mL^{-1}) or algal organic matter (AOM) in Yangshan (YS) lake water-1 (sampled on August 3, 2021) at the MeHg concentration of 0.05 nM (C) or in YS lake water-2 (sampled on November 15, 2022) at the MeHg concentration of 0.001 nM (D). All natural waters were filter-sterilized through 0.2-μm syringe filters before use. Data represent averages from 2–4 replicate samples with error bars showing one standard deviation.

References

1. Parks JM, Johs A, Podar M, Bridou R, Hurt RA, Smith SD*, et al.* The genetic basis for bacterial mercury methylation. *Science* 2013, **339:** 1332-1335.

2. Podar M, Gilmour CC, Brandt CC, Soren A, Brown SD, Crable BR*, et al.* Global prevalence and distribution of genes and microorganisms involved in mercury methylation. *Sci Adv* 2015, **1**(9)**:** e1500675.

3. Mason RP, Reinfelder JR, Morel FMM. Bioaccumulation of mercury and methylmercury. *Water, Air, Soil Pollut.* 1995, **80**(1)**:** 915-921.

4. Chen CY, Driscoll CT, Eagles-Smith CA, Eckley CS, Gay DA, Hsu-Kim H*, et al.* A critical time for mercury science to inform global policy. *Environ. Sci. Technol.* 2018, **52**(17)**:** 9556-9561.

5. Wu P, Zakem EJ, Dutkiewicz S, Zhang Y. Biomagnification of methylmercury in a marine plankton ecosystem. *Environ. Sci. Technol.* 2020, **54**(9)**:** 5446-5455.

6. Zhang Y, Soerensen AL, Schartup AT, Sunderland EM. A global model for methylmercury formation and uptake at the base of marine food webs. *Global Biogeochem. Cycles* 2020, **34**(2)**:** e2019GB006348.

7. Gosnell KJ, Dam HG, Mason RP. Mercury and methylmercury uptake and trophic transfer from marine diatoms to copepods and field collected zooplankton. *Mar. Environ. Res.* 2021, **170:** 105446.

8. Schartup AT, Qureshi A, Dassuncao C, Thackray CP, Harding G, Sunderland EM. A model for methylmercury uptake and trophic transfer by marine plankton. *Environ. Sci. Technol.* 2018, **52**(2)**:** 654-662.

9. Field CB, Behrenfeld MJ, Randerson JT, Falkowski P. Primary production of the biosphere: integrating terrestrial and oceanic components. *Science* 1998, **281:** 237-240.

10. Barkay T, Gu B. Demethylation—The other side of the mercury methylation coin: A critical review. *ACS Environ. Au* 2022, **2**(2)**:** 77-97.

11. Black FJ, Poulin BA, Flegal AR. Factors controlling the abiotic photo-degradation of monomethylmercury in surface waters. *Geochim. Cosmochim. Acta* 2012, **84:** 492-507.

12. Jeremiason JD, Portner JC, Aiken GR, Hiranaka AJ, Dvorak MT, Tran KT*, et al.* Photoreduction of Hg(II) and photodemethylation of methylmercury: the key role of thiol sites on dissolved organic matter. *Environ Sci Process Impacts* 2015, **17**(11)**:** 1892-1903.

13. Tedetti M, Sempéré R. Penetration of ultraviolet radiation in the marine environment. A review. *Photochem. Photobiol.* 2006, **82**(2)**:** 389-397.

14. Li Y, Li D, Song B, Li Y. The potential of mercury methylation and demethylation by 15 species of marine microalgae. *Water Res.* 2022, **215:** 118266.

15. Lu X, Liu Y, Johs A, Zhao L, Wang T, Yang Z*, et al.* Anaerobic Mercury Methylation and Demethylation by Geobacter bemidjiensis Bem. *Environ. Sci. Technol.* 2016, **50**(8)**:** 4366-4373.

16. Lu X, Gu W, Zhao L, Farhan Ul Haque M, DiSpirito AA, Semrau JD*, et al.* Methylmercury uptake and degradation by methanotrophs. *Sci. Adv.*2017, **3:** e1700041.

17. Monperrus M, Tessier E, Amouroux D, Leynaert A, Huonnic P, Donard OFX. Mercury methylation, demethylation and reduction rates in coastal and marine surface waters of the Mediterranean Sea. *Mar. Chem.* 2007, **107**(1)**:** 49-63.

18. Whalin L, Kim E-H, Mason R. Factors influencing the oxidation, reduction, methylation and demethylation of mercury species in coastal waters. *Mar. Chem.* 2007, **107**(3)**:** 278-294.

19. Bravo AG, Le Faucheur S, Monperrus M, Amouroux D, Slaveykova VI. Species-specific isotope tracers to study the accumulation and biotransformation of mixtures of inorganic and methyl mercury by the microalga *Chlamydomonas reinhardtii*. *Environ. Pollut.* 2014, **192:** 212-215.

20. Sharif A, Monperrus M, Tessier E, Bouchet S, Pinaly H, Rodriguez-Gonzalez P*, et al.* Fate of mercury species in the coastal plume of the Adour River estuary (Bay of Biscay, SW France). *Sci. Total Environ.* 2014, **496:** 701-713.

21. Beauvais-Flück R, Slaveykova VI, Cosio C. Transcriptomic and physiological responses of the green microalga *Chlamydomonas reinhardtii* during short-term exposure to subnanomolar methylmercury concentrations. *Environ. Sci. Technol.* 2016, **50**(13)**:** 7126-7134.

22. Beauvais-Flück R, Slaveykova VI, Cosio C. Cellular toxicity pathways of inorganic and methyl mercury in the green microalga Chlamydomonas reinhardtii. *Sci. Rep.* 2017, **7**(1)**:** 8034.

23. Kritee K, Motta LC, Blum JD, Tsui MT-K, Reinfelder JR. Photomicrobial visible light-induced magnetic mass independent fractionation of mercury in a marine microalga. *ACS Earth Space Chem.* 2018, **2**(5)**:** 432-440.

24. Lee C-S, Fisher NS. Microbial generation of elemental mercury from dissolved methylmercury in seawater. *Limnol. Oceanogr.* 2019, **64**(2)**:** 679-693.

25. Cossart T, Garcia-Calleja J, Worms IAM, Tessier E, Kavanagh K, Pedrero Z*, et al.* Species-specific isotope tracking of mercury uptake and transformations by pico-nanoplankton in an eutrophic lake. *Environ. Pollut.* 2021, **288:** 117771.

26. Slaveykova VI, Majumdar S, Regier N, Li W, Keller AA. Metabolomic responses of green alga *Chlamydomonas reinhardtii* exposed to sublethal concentrations of inorganic and methylmercury. *Environ. Sci. Technol.* 2021, **55**(6)**:** 3876-3887.

27. Cossart T, Garcia-Calleja J, Santos JP, Kalahroodi EL, Worms IAM, Pedrero Z*, et al.* Role of phytoplankton in aquatic mercury speciation and transformations. *Environ. Chem.* 2022, **19**(4)**:** 104-115.

28. Gascón Díez E, Loizeau J-L, Cosio C, Bouchet S, Adatte T, Amouroux D*, et al.* Role of settling particles on mercury methylation in the oxic water column of freshwater systems. *Environ. Sci. Technol.* 2016, **50**(21)**:** 11672-11679.

29. Bouchet S, Tessier E, Masbou J, Point D, Lazzaro X, Monperrus M*, et al.* In situ photochemical transformation of Hg species and associated isotopic fractionation in the water column of high-altitude lakes from the Bolivian Altiplano. *Environ. Sci. Technol.* 2022, **56**(4)**:** 2258-2268.

30. Duval B, Tessier E, Kortazar L, Fernandez LA, de Diego A, Amouroux D. Dynamics, distribution, and transformations of mercury species from pyrenean high-altitude lakes. *Environ. Res.* 2023, **216:** 114611.

31. Lee C-S, Fisher NS. Methylmercury uptake by diverse marine phytoplankton. *Limnol. Oceanogr.* 2016, **61:** 1626-1639.

32. Safi C, Zebib B, Merah O, Pontalier P-Y, Vaca-Garcia C. Morphology, composition, production, processing and applications of *Chlorella vulgaris*: A review. *Renewable Sustainable Energy Rev.* 2014, **35:** 265-278.

33. Rastogi RP, Madamwar D, Incharoensakdi A. Bloom dynamics of cyanobacteria and their toxins: Environmental health impacts and mitigation strategies. *Front. Microbiol.* 2015, **6**(1254).

34. Malviya S, Scalco E, Audic S, Vincent F, Veluchamy A, Poulain J*, et al.* Insights into global diatom distribution and diversity in the world's ocean. *Proc. Natl Acad. Sci. USA* 2016, **113:** E1516-E1525.

35. Gu B, Bian Y, Miller CL, Dong W, Jiang X, Liang L. Mercury reduction and complexation by natural organic matter in anoxic environments. *Proc. Natl Acad. Sci. USA* 2011, **108**(4)**:** 1479-1483.

614 36. Hu H, Lin H, Zheng W, Tomanicek SJ, Johs A, Feng X*, et al.* Oxidation and methylation of
615 dissolved elemental mercury by anaerobic bacteria. *Nat. Geosci.* 2013, **6**(9)**:** 751-754.

616 37. Li WKW. Macroecological patterns of phytoplankton in the northwestern North Atlantic
617 Ocean. *Nature* 2002, **419**(6903)**:** 154-157.

618 38. Mason RP, Choi AL, Fitzgerald WF, Hammerschmidt CR, Lamborg CH, Soerensen AL*, et al.*
619 Mercury biogeochemical cycling in the ocean and policy implications. *Environ. Res.* 2012, **119:**
620 101-117.

621 39. Hawkings JR, Linhoff BS, Wadham JL, Stibal M, Lamborg CH, Carling GT*, et al.* Large
622 subglacial source of mercury from the southwestern margin of the Greenland Ice Sheet. *Nat.*
623 *Geosci.* 2021, **14:** 496-502.

624 40. Pickhardt PC, Folt CL, Chen CY, Klaue B, Blum JD. Algal blooms reduce the uptake of toxic
625 methylmercury in freshwater food webs. *Proc. Natl Acad. Sci. USA* 2002, **99:** 4419-4423.

626 41. Xiong J-Q, Kurade MB, Kim JR, Roh H-S, Jeon B-H. Ciprofloxacin toxicity and its co-
627 metabolic removal by a freshwater microalga *Chlamydomonas mexicana*. *J. Hazard. Mater.*
628 2017, **323:** 212-219.

629 42. Zhu Z, Wang S, Zhao F, Wang S, Liu F, Liu G. Joint toxicity of microplastics with triclosan
630 to marine microalgae Skeletonema costatum. *Environ. Pollut.* 2019, **246:** 509-517.

631 43. Wang B, Chen M, Zheng M, Qiu Y. Responses of two coastal algae (*Skeletonema costatum*
632 and *Chlorella vulgaris*) to changes in light and iron levels. *J. Phycol.* 2020, **56**(3)**:** 618-629.

633 44. Guo Z, Tong YW. The interactions between *Chlorella vulgaris* and algal symbiotic bacteria
634 under photoautotrophic and photoheterotrophic conditions. *J. Appl. Phycol.* 2014, **26**(3)**:** 1483-
635 1492.

636 45. Ramanan R, Kim B-H, Cho D-H, Oh H-M, Kim H-S. Algae–bacteria interactions: Evolution,
637 ecology and emerging applications. *Biotechnol. Adv.* 2016, **34**(1)**:** 14-29.

638 46. Christakis CA, Barkay T, Boyd ES. Expanded diversity and phylogeny of mer genes broadens
639 mercury resistance paradigms and reveals an origin for MerA among thermophilic Archaea.
640 *Front. Microbiol.* 2021, **12:** 682605.

641 47. Pak K, Bartha R. Products of Mercury demethylation by Sulfidogens and Methanogens. *Bull.*
642 *Environ. Contam. Toxicol.* 1998, **61**(5)**:** 690-694.

643 48. Schaefer JK, Yagi J, Reinfelder JR, Cardona T, Ellickson KM, Tel-Or S*, et al.* Role of the
644 bacterial organomercury lyase (MerB) in controlling methylmercury accumulation in mercury-
645 contaminated natural waters. *Environ. Sci. Technol.* 2004, **38**(16)**:** 4304-4311.

646 49. Barkay T, Wagner‐Döbler I. Microbial transformations of mercury: Potentials, challenges,
647 and achievements in controlling mercury toxicity in the environment. *Adv. Appl. Microbiol.*
648 2005, **57:** 1-52.

649 50. Griffin HG, Foster TJ, Silver S, Misra TK. Cloning and DNA sequence of the mercuric- and
650 organomercurial-resistance determinants of plasmid pDU1358. *Proc. Natl Acad. Sci. USA* 1987,
651 **84:** 3112-3116.

652 51. Johs A, Harwood IM, Parks JM, Nauss RE, Smith JC, Liang L*, et al.* Structural
653 characterization of intramolecular Hg^{2+} transfer between flexibly linked domains of mercuric
654 ion reductase. *J. Mol. Biol.* 2011, **413**(3)**:** 639-656.

655 52. Lian P, Guo H-B, Riccardi D, Dong A, Parks JM, Xu Q*, et al.* X-ray Structure of a Hg^{2+}
656 complex of mercuric reductase (MerA) and quantum mechanical/molecular mechanical study
657 of Hg^{2+} transfer between the C-Terminal and buried catalytic site cysteine pairs. *Biochemistry*
658 2014, **53**(46)**:** 7211-7222.

659 53. Pérez-Pérez ME, Lemaire SD, Crespo JL. Reactive oxygen species and autophagy in plants
660 and algae. *Plant Physiol.* 2012, **160**(1)**:** 156-164.

661 54. Diaz JM, Plummer S. Production of extracellular reactive oxygen species by phytoplankton:
662 past and future directions. *J. Plankton Res.* 2018, **40**(6)**:** 655-666.

663 55. Zhang T, Hsu-Kim H. Photolytic degradation of methylmercury enhanced by binding to
664 natural organic ligands. *Nat. Geosci.* 2010, **3**(7)**:** 473-476.

665 56. Sheng F, Ling J, Hong R, Jin X, Wang C, Zhong H*, et al.* A new pathway of
666 monomethylmercury photodegradation mediated by singlet oxygen on the interface of sediment
667 soil and water. *Environ. Pollut.* 2019, **248:** 667-675.

668 57. Telfer A, Dhami S, Bishop SM, Phillips D, Barber J. .beta.-carotene quenches singlet oxygen
669 formed by isolated photosystem II reaction centers. *Biochemistry* 1994, **33**(48)**:** 14469-14474.

670 58. Han X, Li Y, Li D, Liu C. Role of free radicals/reactive oxygen species in MeHg
671 photodegradation: Importance of utilizing appropriate scavengers. *Environ. Sci. Technol.* 2017,
672 **51**(7)**:** 3784-3793.

673 59. Garcia-Calleja J, Cossart T, Pedrero Z, Santos JP, Ouerdane L, Tessier E*, et al.* Determination
674 of the intracellular complexation of inorganic and methylmercury in cyanobacterium
675 *Synechocystis sp.* PCC 6803. *Environ. Sci. Technol.* 2021, **55**(20)**:** 13971-13979.

676 60. Rezayian M, Niknam V, Ebrahimzadeh H. Oxidative damage and antioxidative system in
677 algae. *Arch. Toxicol.* 2019, **6:** 1309-1313.

61. Wolfe GV, Strom SL, Holmes JL, Radzio T, Olson MB. Dimethylsulfoniopropionate cleavage by marine phytoplankton in response to mechanical, chemical, or dark stress. *J. Phycol.* 2002, **38**(5)**:** 948-960.

62. Lei P, Zhang J, Zhu J, Tan Q, Kwong RWM, Pan K*, et al.* Algal organic matter drives methanogen-mediated methylmercury production in water from eutrophic shallow lakes. *Environ. Sci. Technol.* 2021, **55**(15)**:** 10811-10820.

63. Zhong H, Wang W-X. Controls of dissolved organic matter and chloride on mercury uptake by a marine diatom. *Environ. Sci. Technol.* 2009, **43**(23)**:** 8998-9003.

64. Gorski PR, Armstrong DE, Hurley JP, Krabbenhoft DP. Influence of natural dissolved organic carbon on the bioavailability of mercury to a freshwater alga. *Environ. Pollut.* 2008, **154**(1)**:** 116-123.

65. Ho JC, Michalak AM, Pahlevan N. Widespread global increase in intense lake phytoplankton blooms since the 1980s. *Nature* 2019, **574**(7780)**:** 667-670.

66. Grégoire DS, Poulain AJ. A little bit of light goes a long way: the role of phototrophs on mercury cycling. *Metallomics* 2014, **6**(3)**:** 396-407.

67. Chen Q, Han H, Zhai S, Hu W. Influence of solar radiation and water temperature on chlorophyll-a levels in lake Taihu. *Acta Scientiae Circumstantiae* 2009, **29:** 199-206.

68. Trumpickas J, Shuter BJ, Minns CK, Cyr H. Characterizing patterns of nearshore water temperature variation in the North American Great Lakes and assessing sensitivities to climate change. *J. Great Lakes Res.* 2015, **41**(1)**:** 53-64.

69. Toffolon M, Piccolroaz S, Calamita E. On the use of averaged indicators to assess lakes' thermal response to changes in climatic conditions. *Environ. Res. Lett.* 2020, **15**(3)**:** 034060.

70. Zhang T, Zhou W, Lin X, Khan MR, Deng S, Zhou M*, et al.* Light-up RNA aptamer signaling-CRISPR-Cas13a-based mix-and-read assays for profiling viable pathogenic bacteria. *Biosens. Bioelectron.* 2021, **176:** 112906.

71. dos Santos HRM, Argolo CS, Argôlo-Filho RC, Loguercio LL. A 16S rDNA PCR-based theoretical to actual delta approach on culturable mock communities revealed severe losses of diversity information. *BMC Microbiol.* 2019, **19**(1)**:** 74.

72. Mu L, Zhou Q, Zhao Y, Liu X, Hu X. Graphene oxide quantum dots stimulate indigenous bacteria to remove oil contamination. *J. Hazard. Mater.* 2019, **366:** 694-702.

73. An J, Zhang L, Lu X, Pelletier DA, Pierce EM, Johs A*, et al.* Mercury uptake by *Desulfovibrio desulfuricans* ND132: Passive or active? *Environ. Sci. Technol.* 2019, **53**(11)**:** 6264-6272.

74. The UniProt Consortium. UniProt: a worldwide hub of protein knowledge. *Nucleic Acids Res.* 2018, **47**(D1)**:** D506-D515.

75. Grigoriev IV, Nordberg H, Shabalov I, Aerts A, Cantor M, Goodstein D*, et al.* The genome portal of the Department of Energy Joint Genome Institute. *Nucleic Acids Res.* 2011, **40**(D1)**:** D26-D32.

76. Nordberg H, Cantor M, Dusheyko S, Hua S, Poliakov A, Shabalov I*, et al.* The genome portal of the Department of Energy Joint Genome Institute: 2014 updates. *Nucleic Acids Res.* 2014, **42**(D1)**:** D26-D31.

77. Guarnieri MT, Levering J, Henard CA, Boore JL, Betenbaugh MJ, Zengler K*, et al.* Genome sequence of the Oleaginous Green Alga, *Chlorella vulgaris* UTEX 395. *Front. Bioeng. Biotechnol.* 2018, **6**(37): 1-2.

78. Altschul SF, Gish W, Miller W, Myers EW, Lipman DJ. Basic local alignment search tool. *J. Mol. Biol.* 1990, **215**(3)**:** 403-410.

79. Sievers F, Wilm A, Dineen D, Gibson TJ, Karplus K, Li W*, et al.* Fast, scalable generation of high-quality protein multiple sequence alignments using Clustal Omega. *Mol. Syst. Biol.* 2011, **7**(1)**:** 539.

80. Waterhouse AM, Procter JB, Martin DMA, Clamp M, Barton GJ. Jalview Version 2-a multiple sequence alignment editor and analysis workbench. *Bioinform.* 2009, **25**(9)**:** 1189-1191.

81. Burns JM, Cooper WJ, Ferry JL, King DW, DiMento BP, McNeill K*, et al.* Methods for reactive oxygen species (ROS) detection in aqueous environments. *Aquat. Sci.* 2012, **74**(4)**:** 683-734.

82. Gui S, Huang Y, Hu F, Jin Y, Zhang G, Zhang D*, et al.* Bioinspired peptide for imaging Hg^{2+} distribution in living cells and zebrafish based on coordination-mediated supramolecular assembling. *Anal. Chem.* 2018, **90**(16)**:** 9708-9715.

83. Prasad A, Sedlářová M, Pospíšil P. Singlet oxygen imaging using fluorescent probe Singlet Oxygen Sensor Green in photosynthetic organisms. *Sci. Rep.* 2018, **8**(1)**:** 13685.

84. Damas-Souza DM, Nunes R, Carvalho HF. An improved acridine orange staining of DNA/RNA. *Acta Histochem.* 2019, **121**(4)**:** 450-454.

85. Flors C, Fryer MJ, Waring J, Reeder B, Bechtold U, Mullineaux PM*, et al.* Imaging the production of singlet oxygen in vivo using a new fluorescent sensor, Singlet Oxygen Sensor Green. *J. Exp. Bot.* 2006, **57**(8)**:** 1725-1734.

741 86. Bolte S, Cordelieres FP. A guided tour into subcellular colocalization analysis in light
742 microscopy. *J. Microsc.* 2006, **224**(3)**:** 213-232.

743 87. French AP, Mills S, Swarup R, Bennett MJ, Pridmore TP. Colocalization of fluorescent
744 markers in confocal microscope images of plant cells. *Nat. Protoc.* 2008, **3**(4)**:** 619-628.

745 88. Liang X, Lu X, Zhao J, Liang L, Zeng EY, Gu B. Stepwise reduction approach reveals mercury
746 competitive binding and exchange reactions within natural organic matter and mixed organic
747 ligands. *Environ. Sci. Technol.* 2019, **53**(18)**:** 10685-10694.

748

749

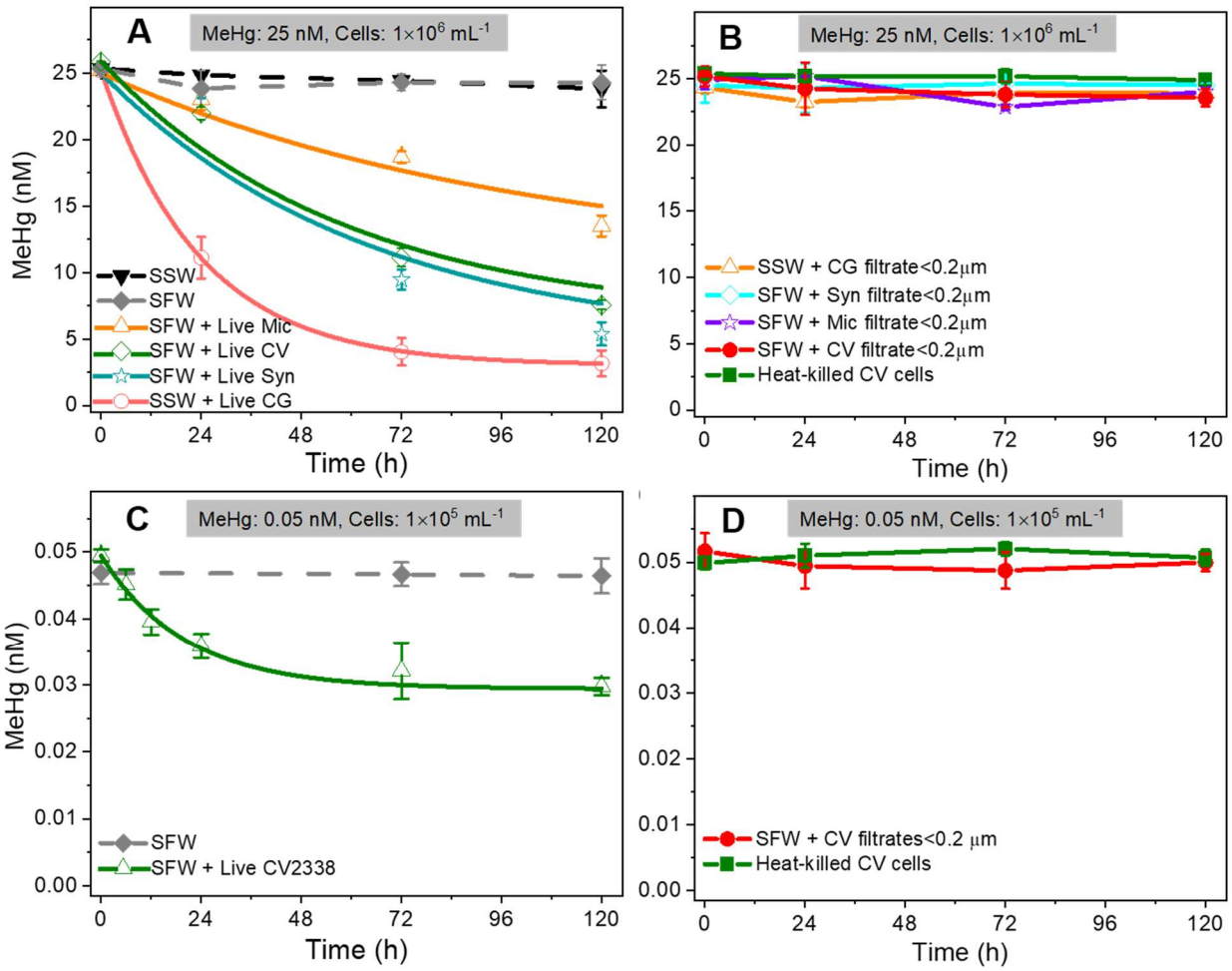

750

751 **Fig. 1.**

752

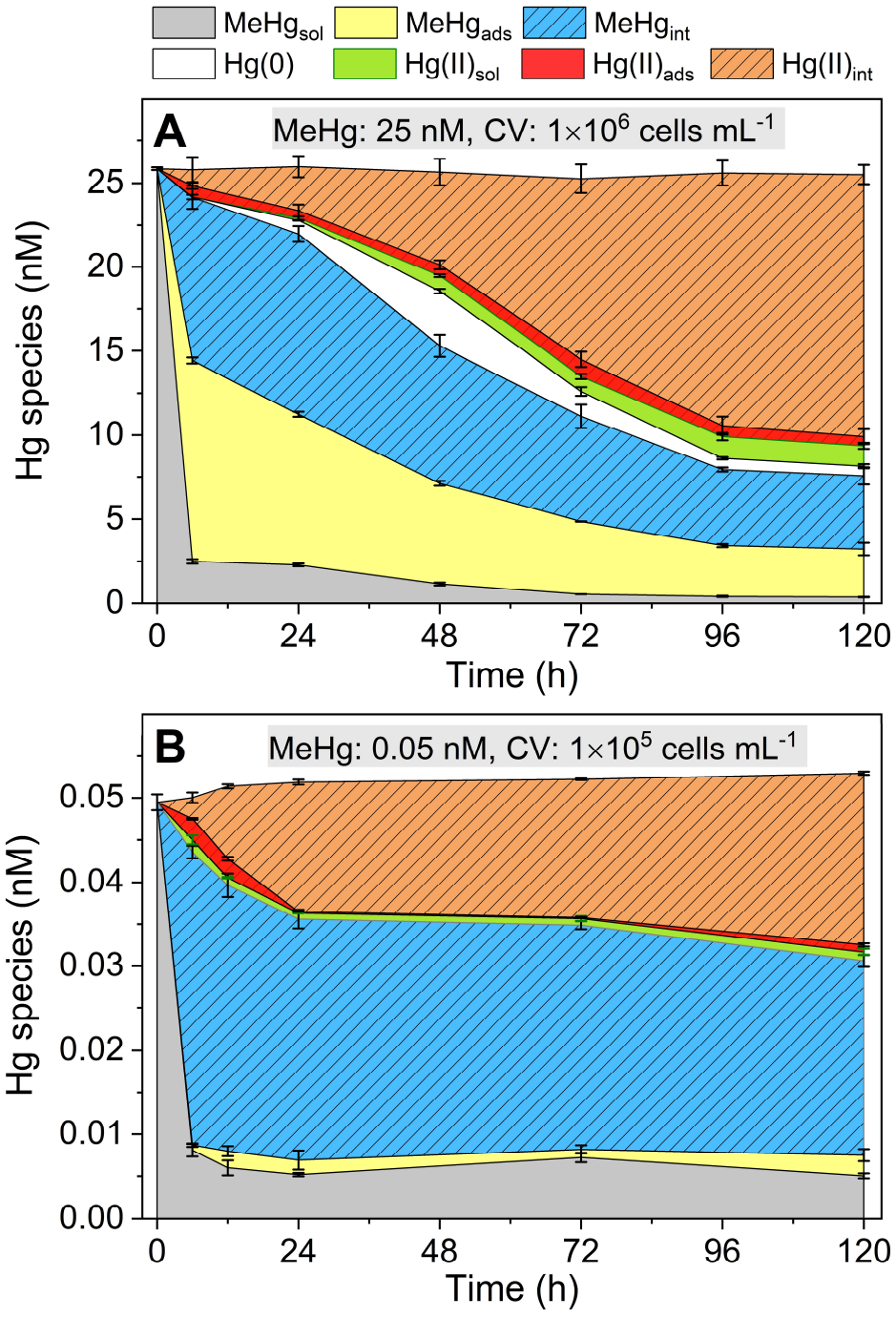

753

754 **Fig. 2.**

755

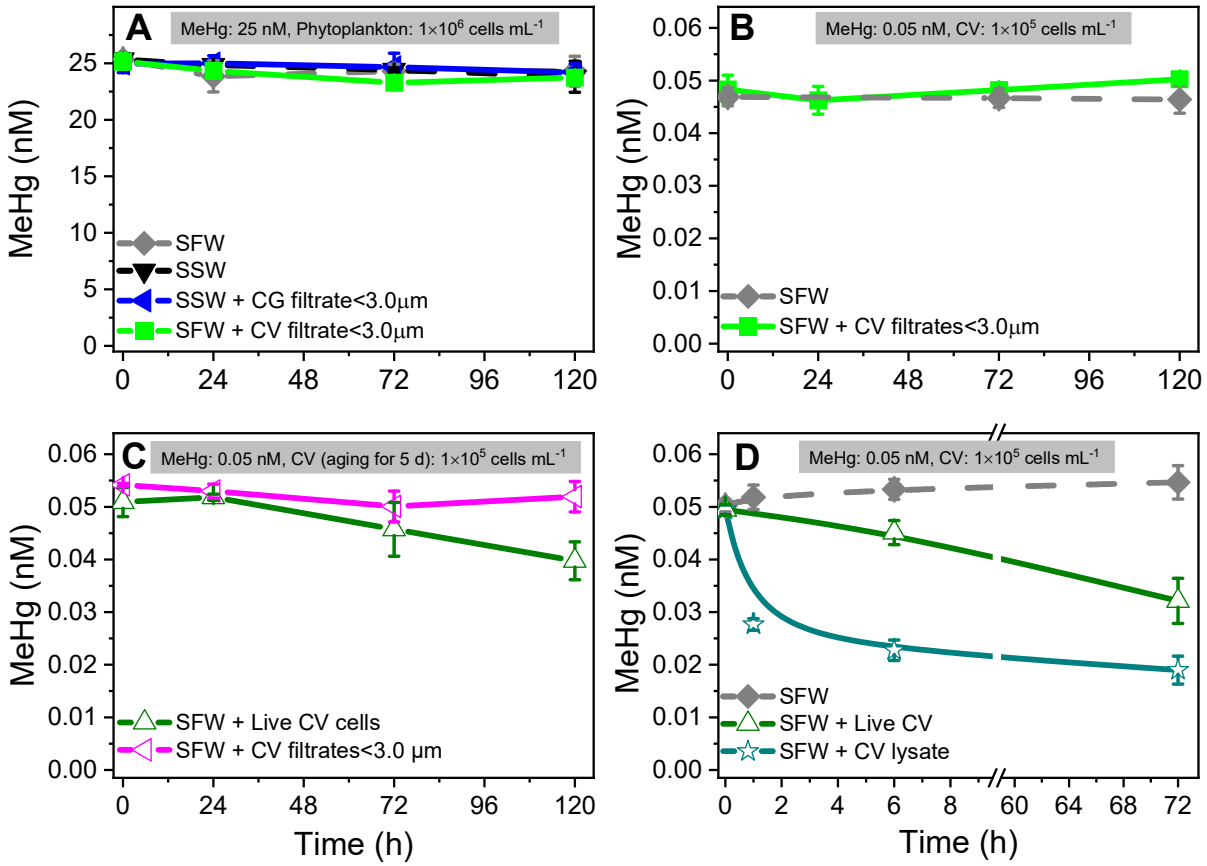
A
MeHg: 25 nM, Phytoplankton: 1×10^6 cells mL^-1
SFW
SSW
SSW + CG filtrate<3.0μm
SFW + CV filtrate<3.0μm
B
MeHg: 0.05 nM, CV: 1×10^5 cells mL^-1
SFW
SFW + CV filtrates<3.0μm
C
MeHg: 0.05 nM, CV (aging for 5 d): 1×10^5 cells mL^-1
SFW + Live CV cells
SFW + CV filtrates<3.0 μm
D
MeHg: 0.05 nM, CV: 1×10^5 cells mL^-1
SFW
SFW + Live CV
SFW + CV lysate
MeHg (nM)
Time (h)

Fig. 3.

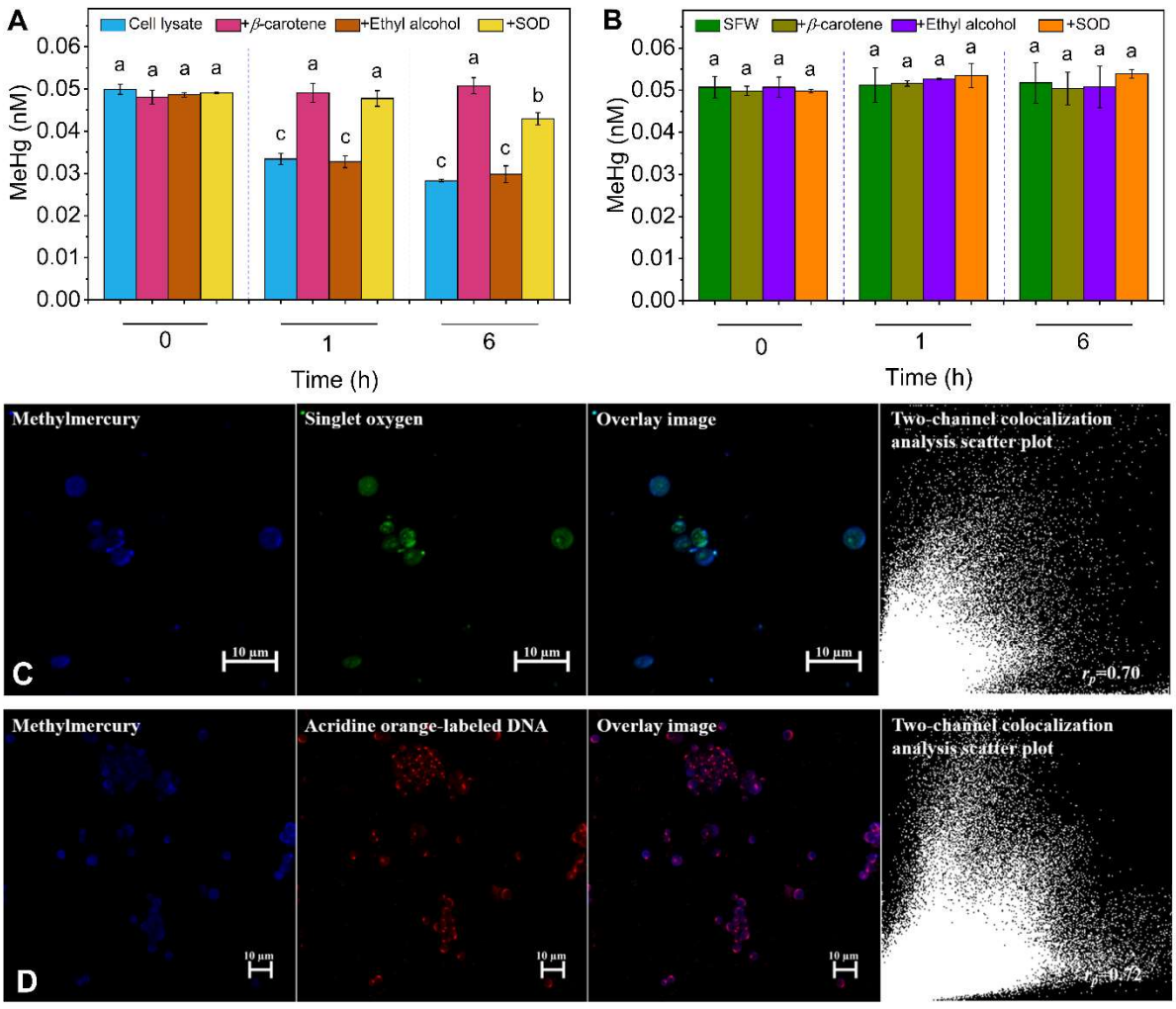
A
Cell lysate
+β-carotene
+Ethyl alcohol
+SOD
MeHg (nM)
Time (h)
B
SFW
+β-carotene
+Ethyl alcohol
+SOD
MeHg (nM)
Time (h)
Methylmercury
Singlet oxygen
Overlay image
Two-channel colocalization analysis scatter plot
C
Methylmercury
Acridine orange-labeled DNA
Overlay image
Two-channel colocalization analysis scatter plot
D

Fig. 4.

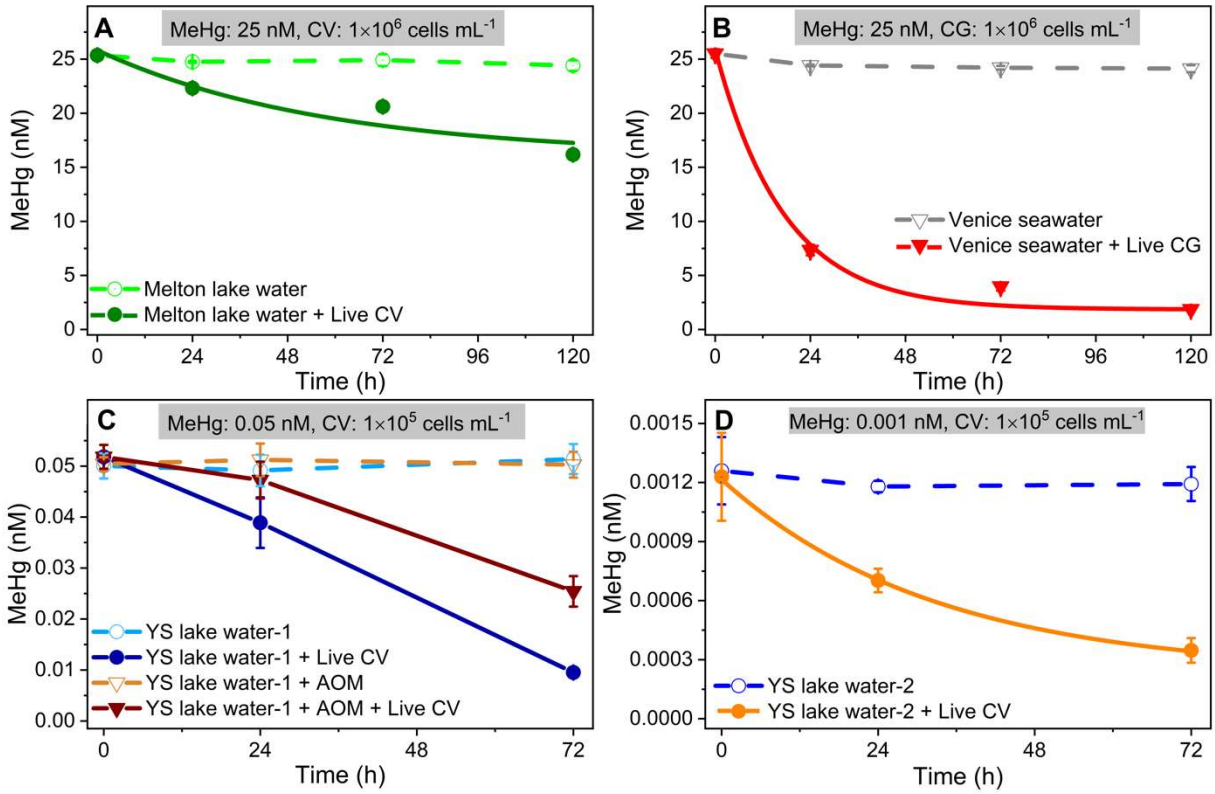
A
MeHg: 25 nM, CV: 1×10^6 cells mL^-1
MeHg (nM)
Time (h)
Melton lake water
Melton lake water + Live CV
B
MeHg: 25 nM, CG: 1×10^6 cells mL^-1
Venice seawater
Venice seawater + Live CG
C
MeHg: 0.05 nM, CV: 1×10^5 cells mL^-1
YS lake water-1
YS lake water-1 + Live CV
YS lake water-1 + AOM
YS lake water-1 + AOM + Live CV
D
MeHg: 0.001 nM, CV: 1×10^5 cells mL^-1
YS lake water-2
YS lake water-2 + Live CV

Fig. 5.